Persistent Shallow Background Microseismicity on Hekla Volcano, Iceland: A Potential Monitoring Tool

Eva P. S. Eibl[1] (eva.eibl@ucdconnect.ie), Christopher J. Bean[1], Kristín Vogfjörd [2], Aoife Braiden[1]
1: Seismology Laboratory, School of Geological Sciences, University College Dublin, Belfield, Dublin 4, Ireland
2: Icelandic Meteorological Office, Bústaðavegi 7 - 9, 108 Reykjavik, Iceland

1 Abstract

Hekla is one of Iceland's most active volcanoes. Since 1970 it has erupted four times with a period of quiescence of 14 years since the last eruption. We detected persistent levels of background microseismicity with a temporary seismic network in autumn 2012. An amplitude based as well as an arrival-time based location method was applied to two populations of events and located them at shallow depths on the northern flank, close to the summit. This seismicity has not been identified previously by the permanent seismic network in Iceland as it is below its detection threshold. The detected events were either short, higher frequency events with distinct arrivals located beneath the summit on the northern flank of Hekla or longer, emergent, lower frequency events about 4 km northeast of the summit at 200âĂŞ400 m depth below the surface. Estimated moment magnitudes were MW = -1.1 to -0.1 and MW = -0.9 to -0.0 and local magnitudes ML = -0.5 to +0.3 and ML = -0.3 to +0.3, respectively. This seismicity does not show any correlation with gas output but is located at the steepest slopes of the edifice. Hence we suggest that the current shallow microseismicity at Hekla is structurally controlled. This offers a possible opportunity of using near summit microseismicity as a tool for monitoring emerging unrest at Hekla. Microseismicity rates will be very sensitive to small stress perturbations due to magma migration at depth. Currently in the absence of microseismicity monitoring, Hekla switches from apparently quiescent to fully eruptive on the order of only 1 h.

2 Introduction

Hekla is one of Iceland's most active volcanoes, located on the Mid-Atlantic plate margin. Its activity is related to its position at the connection between the South Iceland Seismic Zone striking east-west and the Eastern Volcanic Zone striking north-south (Einarsson, 1991). Hekla is elongated in WSW-ENE direction with similarly trending fractures through its summit. Previous eruptions had a repose time of about 60 years before 1970 and about 10 years after 1970 (Soosalu and Einarsson, 1997) with eruptions in 1970 (Einarsson and Björnsson, 1976), 1980/81 (Grönvold et al., 1983), 1991 (Gudmundsson et al., 1992) and its latest in 2000 (e.g. Höskuldsson et al. (2007); Soosalu et al. (2005)). After an eruption on Heimaey Island offshore south Iceland in 1973 (Thórarinsson et al., 1973) a permanent, analogue seismic network was set up in South Iceland including a station 31 km southwest of Hekla in 1974 (Einarsson and Björnsson, 1987). This station was the closest to Hekla until 1982 when an additional permanent station 22 km west of Hekla was installed (Einarsson and Björnsson, 1987). Those stations recorded tremor during and shortly before the subsequent eruptions which was analysed in further detail (Grönvold et al., 1983). Detailed studies of the earthquakes around Hekla were based on the network operated by the Icelandic Meteorological Office (IMO) that has been recording since the beginning of 1990. Currently the closest permanent seismometer is a digital, 3-component Lennartz 5s instrument in Haukadalur 15 km west of Hekla (see e.g. Jakobsdóttir (2008)). From March 1982 (Einarsson and Björnsson, 1987) until 2010 (pers. comm. Páll Einarsson, May 2014) an analogue, vertical-component seismometer was additionally operated 2 km north of the summit. Two other temporary digital, 3-component, broadband stations are operated by IMO since late 2011/ early 2012 about 4 km north and 6.5 km south of Hekla (pers. comm. Martin Hensch, May 2014).

It has been observed that seismic activity at Hekla is strongly linked to its eruptions (e.g. Einarsson (1991)). The visual beginning of an eruption is accompanied by low-frequency (0.5 - 1.5 Hz with dominant peaks at 0.7 - 0.9) volcanic tremor that decreases the detection threshold for earthquakes classified as high-frequency and low-frequency in Soosalu et al. (2005). Those high and low-frequency events comprise the sparse background activity (Soosalu and Einarsson, 2002; Soosalu et al., 2005). Earthquake signals containing only low-frequencies have been observed at Hekla during inter-eruption periods. They have clear P and S wave onsets, occurred in the 8 - 14 km depth range and were interpreted as tectonic events with low stress drop (Soosalu and Einarsson, 1997). The high-frequency earthquakes were observed during eruptions and a few months before or after an eruption. They occur in the 8 - 12 km depth range and are also interpreted as tectonic earthquakes, but requiring higher strain relative to the low-frequency events (Soosalu et al., 2005).

Seismic precursors to the four eruptions since 1970 were detected 25, 23, 28 and about 80 minutes (Einarsson and Björnsson, 1976; Grönvold et al., 1983; Gudmundsson et al., 1992; Soosalu et al., 2005) before the visible onset of the eruption. They were thought to be related to movement of magma. In 2000, for instance, the seismicity started gradually, growing in event frequency and intensity (M_L -0.5 to +2.1) over a timescale of several tens of minutes. 80 to 45 minutes before the eruption some of the events could be located in the depth range of 0 - 4 km. In the next ten minutes the seismicity was located at up to 6 km depth and from 35 minutes before the eruption they occurred in up to 14 km depth mainly in 4 - 9 km depth. Most of the events also clustered north of the main fissure on the summit of Hekla. With the beginning of the eruption the earthquakes in the swarm became more infrequent and decreased in intensity (Soosalu et al., 2005). When the seismicity reached 6 km depth the first contraction signal was observed at the nearest strainmeter at 15 km distance (Sturkell et al., 2013). The contraction rate increased until the start of the eruption. During previous eruptions a similar behaviour was observed. The first seismicity was detected less than half an hour before the eruption at the same time as strainmeters recorded a contraction signal (or expansion depending on the location of the strainmeter) (Linde et al., 1993; Gudmundsson et al., 1992).

Before and after the most recent eruption in 2000 an inflation of an area with a radius of 20 km around Hekla was observed. Shortly before the eruption in 2000 the ground surface south of the eruptive fissure deformed upwards, north of the fissure it deformed downwards. This was probably linked to the intrusion of a dike (Ofeigsson et al., 2011). A GPS study (Geirsson et al., 2012) also detected an inflation signal at Hekla. This study suggests that the observed inflation continued at least until 2010 or 2011.

In summary (i) Hekla is likely still in an inflating phase. (ii) Previous studies have shown that significant levels of seismicity have only been detected on the order of one hour (or less) prior to eruptions. (iii) For these earthquakes three to four times more events were detected at a temporary station ca. 2 km north of the summit in comparison to permanent instrumentation 15 km to the west (IMO station) (Soosalu and Einarsson, 1997, 2002; Soosalu et al., 2005).

In this paper we find significant levels of microseismicity using a temporary deployment of five broadband stations in the summit region (August to October 2012). We suggest that such microseismicity might be used to track low level strain fluctuations. Due to the short warning periods ahead of previous eruptions, the characterisation of level, location, size and process of this seismic activity is important from a hazard perspective. We undertake an analysis of these events using a standard amplitude and an arrival-time based location method. The paper describes event characteristics, location estimates and magnitudes. Locations are interpreted in the context of synthetic simulations, deformation and gas observations.

3 Seismic network on Hekla

We augmented the IMO network from August until October 2012 with five Güralp 6TD (30 s - 100 Hz) sensors on the summit and the eastern flank of Hekla volcano. The first instrument became operational on August, 9th. Data sampled at 100 Hz were stored locally until the instruments were decommissioned on October, 10th. The instrument locations are given in figure 1, their coordinates in table 1. The network was configured with a focus on event detection and accessibility of the site. Locations could be improved with a different geometry and effects are discussed further in section 5.2. The distances between the stations vary between 1 and 4 km. They were buried up to 20 cm deep in unconsolidated volcanic material which was frozen soon after the station deployment.

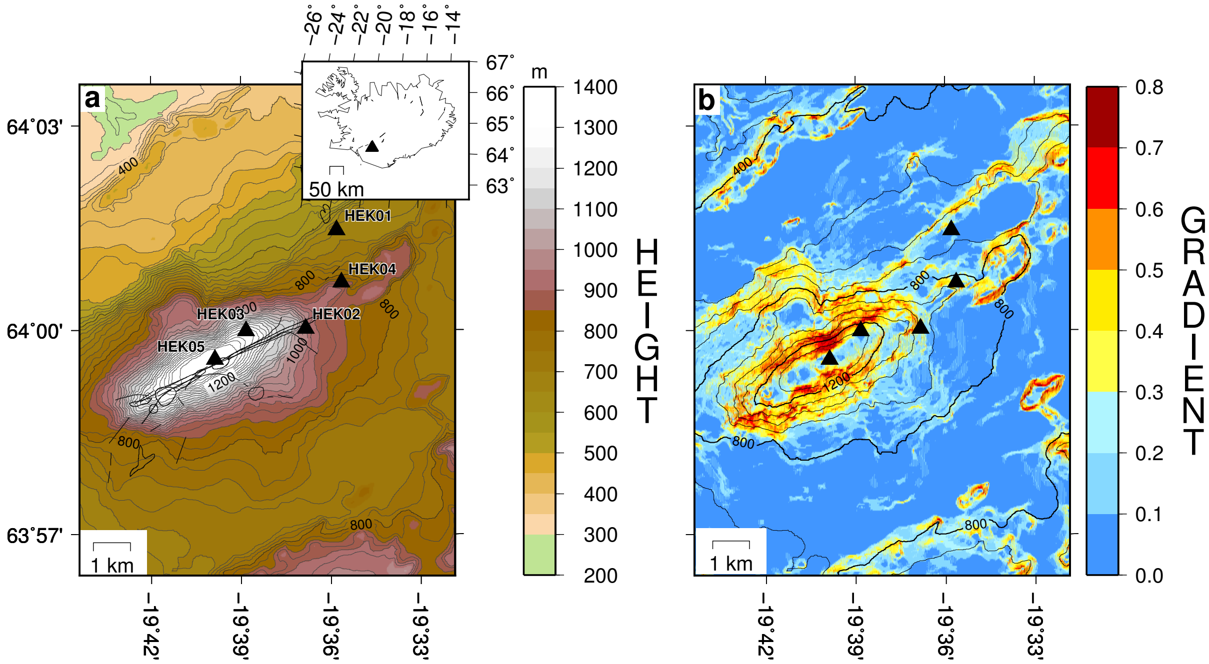

Figure 1: (a) The topography of Hekla volcano and the locations of the seismometers (black triangles). Thin black lines indicate the eruptive fissures of the eruptions in 1970, 1980/81, 1991 and 2000 Höskuldsson et al. (2007). (b) Maximum gradient of the topography indicating the steepest slopes and highlighting the elongation of Hekla along the main eruptive fissures at the summit.

Station	HEK05	HEK03	HEK02	HEK04	HEK01
Station coordinates	63.99281 N 19.66449 W	63.99973 N 19.64707 W	64.00353 N 19.61382 W	64.011646 N 19.593963 W	64.02444 N 19.59652 W
Site correction factor in the 4 - 7 Hz band	1.378350	0.663770	0.851536	0.776647	1.0
Site correction factor in the 7 - 10 Hz band	0.750484	0.360419	0.232864	0.341289	1.0

Table 1: Coordinates and site correction factors at the different stations in the 4 - 7 Hz and 7 - 10 Hz band derived from 53 regional events.

4 Observations

The seismic background activity detected in August to October 2012 consists of two apparently different types of events with different frequency content, signal lengths and onsets. We refer to them as type 1 and type 2 events and show their occurrence in a seven week period in figure 2. The events were picked automatically with a STA/LTA filter that triggered only when an event was visible on at least three seismic stations. Type 1 and type 2 events were visually identified based on their signal length and frequency content. The vertical lines in figure 2 indicate times when seismometers started or stopped recording. All instruments were deployed within three days. Data gaps occurred in late September due to loss of power from snow and ice covering the solar panels. The number next to them corresponds to the number of recording seismometers. If there is a correlation between the number of type 1 and type 2 events it is weak and we do not regard it as significant. Station availability affected the detection threshold and local power failures generally led to an underestimation of the numbers of micro-earthquakes e.g. in late September.

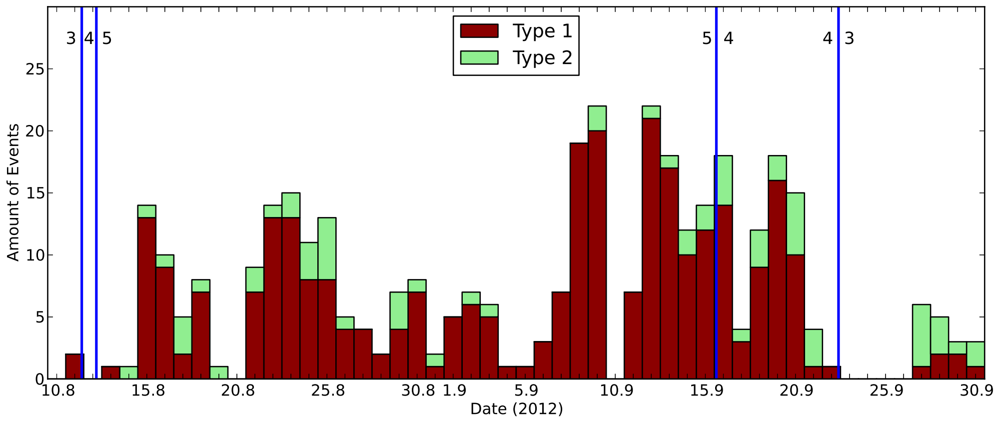

Figure 2: Occurrence of the type 1 and type 2 events during August and September 2012. The vertical lines indicate a change in the number of operational seismometers given by the number.

4.1 Type 1 Events

The shortest events we detected are 3 - 4 s long in duration, have distinct onsets and energy between 3 and 20 Hz, mostly around 10 Hz at the station with the strongest and shortest signal (figure 3a). 85% of the events are earliest (by up to 1 s) at HEK03 (see figure 1) and about 15% are earliest at HEK05. Some events are barely visible or not visible on HEK01 where noise levels are slightly higher.
Different seismic phases cannot be identified, possibly due to close proximity to the source. Soosalu et al. (2005) identified clear P and S phase onsets in events which were recorded at 15 km distance from Hekla. They were classified as high- or low-frequency events, came from the same region as events identified here but had significantly higher amplitudes and associated signal to noise ratio (S/N). Figure 3 shows the three components of a typical event on two different stations and their spectra and spectrogram of the vertical component. Note the significantly lower frequency content on HEK02 although it is only 1.6 km away from HEK03.

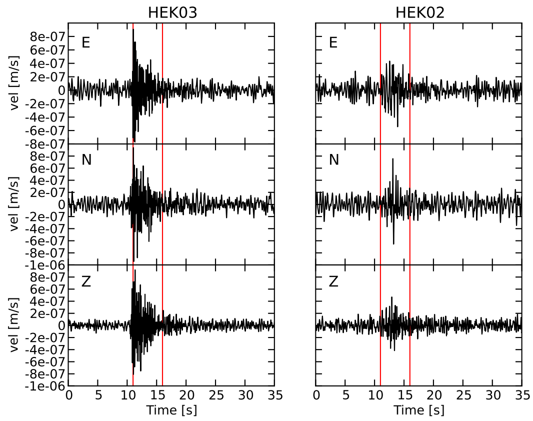

(a) 1 - 20 Hz

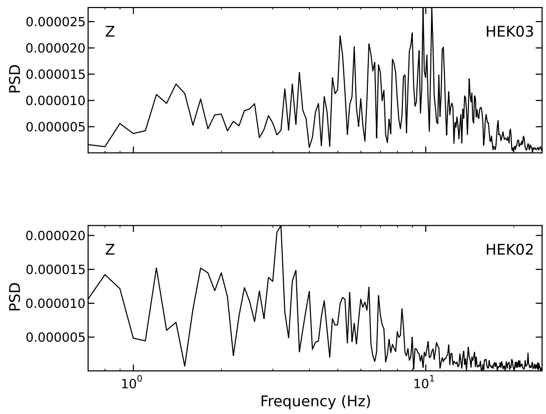

(b) 0.7 - 30 Hz

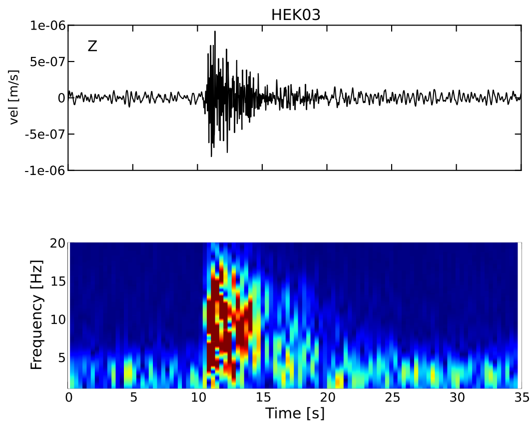

(c) 1 - 20 Hz

Figure 3: A typical 1 - 20 Hz filtered type 1 event which occurred on August 26^{th}, 2012 at 5:52:19. (a) Instrument corrected seismograms on HEK02 and HEK03 on all three components show the earlier arrival on HEK03. The portion of the signal between the vertical red lines was used in the intensity location method. (b) Spectrum of the vertical component at HEK02 and HEK03 showing the high-frequency attenuation on HEK02. (c) Instrument corrected vertical component seismogram and spectrogram of the event at HEK03.

4.2 Type 2 Events

The type 2 events (figure 4) are mostly 10 to 30 s long in duration and emergent. The station closest to the source records frequencies between 1 and 14 Hz with most of the energy being between 2 and 5 Hz. Due to their emergent nature it is not possible to visually observe on which station the event arrives first. Figure 4 shows a typical event recorded on HEK01 and HEK03 on all three components and their spectra and spectrogram. In contrast to type 1 events, type 2 events have a slightly higher S/N and a higher absolute amplitude. Their frequency content is also lower while their duration in time is longer. The diffuse nature and longer duration might be a propagation effect i.e. caused by scattering if the events occurred outside our station network, at greater distances than type 1 events. This might also imply that these events resemble the type 1 events but are slightly bigger in amplitude and occurred farther away from the station. The similar distance travelled from source to the station might be the reason for the similar spectral content at different stations in contrast to the spectral differences observed for type 1 events. In order to improve the locations we considered stacking but as our events do not form families this was not possible.

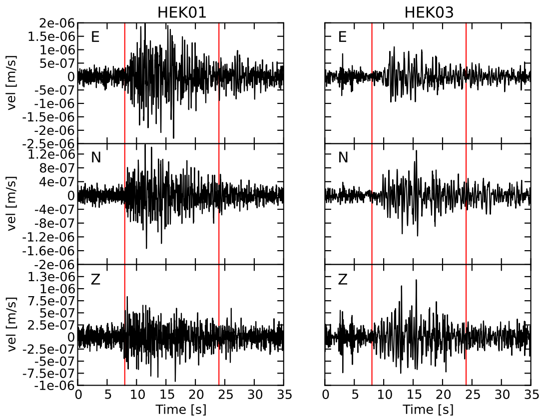

(a) 1 - 20 Hz

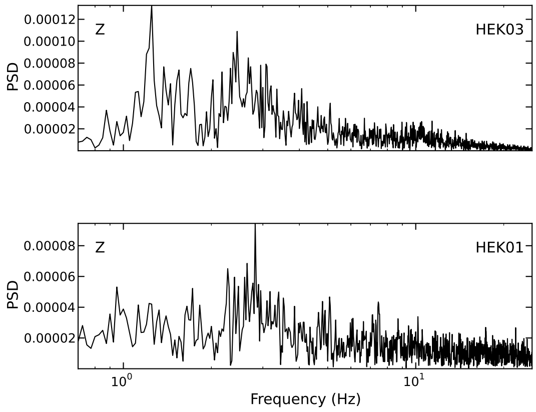

(b) 0.7 - 30 Hz

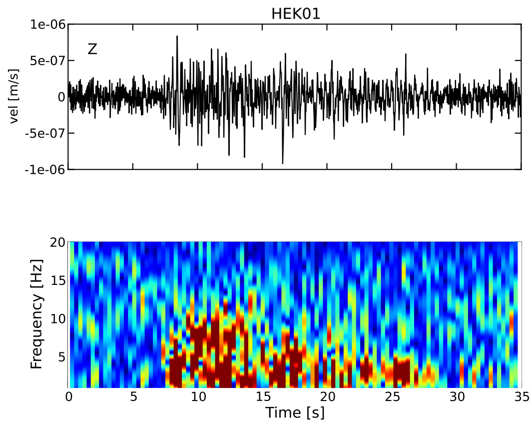

(c) 1 - 20 Hz

Figure 4: A typical 1 - 20 Hz filtered type 2 event which occurred on August 29th, 2012 at 19:01:13. Subfigures as in figure 3. Note the lower frequency content, the emergent onset and longer duration in comparison to the type 1 events.

We have checked the nearest permanent IMO station 15 km west of Hekla for the type 1 and 2 events detected by our network. None of the type 1 events were recorded and about 10% of type 2 events are weakly visible. On the temporary stations at 4 km and 6.5 km distance only 26 type 2 events and no type 1 events could be detected due to data gaps and low signal to noise ratios respectively.

5 Event Locations: Methodology

Arrival-time methods cannot be used for determining locations of our entire database as most of our events are either emergent or have onsets that are often hidden in noise. We based our locations on the intensity location method described in (Taisne et al., 2011) which is based on a study of Battaglia and Aki (2003). In this method the intensity ratios for all station pairs are calculated using the median of the absolute value of the Hilbert Transform of the instrument corrected seismogram. These intensity ratio pairs are then compared with the expected intensity ratios assuming a source at a grid point in a predefined 3D grid:

$$\frac{I_i(r_i)}{I_j(r_j)} = e^{\frac{\pi \cdot f}{Q \cdot \beta} \cdot (r_j - r_i)} \cdot \left(\frac{r_j}{r_i}\right)^n \tag{5.1}$$

where I_i and I_j indicate the amplitudes of the signal at station i and j, r_i and r_j the distance between the source and seismometer i and j, f the dominant frequency of the signal, Q the quality factor for attenuation and β the wave velocity in m/s. n is set to 0.5 for surface waves and 1 for body waves. For n=0.5 the distance r_i is only calculated with respect to x and y as we assume a source on the surface. For n=1 we inverted for x, y and depth (see also Battaglia and Aki (2003)).
To calculated the error percentage (RES) of each grid point the square root of the sum of the squared absolute errors between the observed and calculated intensity ratios divided by the sum of the squared observed intensity ratios is calculated (Battaglia et al., 2005):

$$RES = 100 \cdot \sqrt{\frac{\sum_i \sum_{j>i} \left(\frac{I_{isyn}(r_i)}{I_{jsyn}(r_j)} - \frac{I_i(r_i)}{I_j(r_j)}\right)^2}{\sum_i \sum_{j>i} \left(\frac{I_i(r_i)}{I_j(r_j)}\right)^2}} \tag{5.2}$$

Assumptions are that there is only one source at a given time, that for one event each station record is dominated by the same seismic phase and that each station has the same quality. Noise or a station with a bad fit will lead to a low error percentage and worsen the result. Equation 5.2 is a far field approximation and might create errors for the events closest to the stations especially in the lower frequency band. S waves will have wavelengths of around 360 m in the lower frequency band and 235 m in the higher frequency band. The grid point with the minimum percentage error is assumed as source. This method was previously used to estimate size, length and velocity of pyroclastic flows (Jolly et al., 2002), locate volcanic tremor (Battaglia et al., 2005; Battaglia and Aki, 2003), VT, long-period events (Battaglia and Aki, 2003) and non-volcanic tremor in subduction zones (Husker et al., 2012) and track lahars (Kumagai et al., 2009). Locations were initially either visually confirmed by rocks, flow deposits or eruptive vents or by locations from another location method. Problems with the locations were attributed to more than one active source, anisotropically radiated seismic energy or trapped seismic energy (Jolly et al., 2002), saturation problems at the stations, low signal to noise ratios (Battaglia et al., 2005) and heterogeneities or a magma chamber in the wave path (Battaglia and Aki, 2003).

5.1 Data processing

Altogether, 210 type 1 and 40 type 2 events recorded by 5 stations were located. As a first processing step the seismogram of each event was corrected for the instrument response

and filtered to the 4 - 7 Hz or 7 - 10 Hz frequency band. We chose those frequency bands based on the spectral signal strength and isotropic radiation effects at frequencies above 5 Hz (Kumagai et al., 2010).
In order to perform site corrections we calculated coda amplitudes for 53 regional events. Coda waves are routinely used for site amplification estimations (Kumagai et al., 2009; Battaglia and Aki, 2003; Aki and Ferrazzini, 2000b). The regional events occurred in 15 to 150 km distance from Hekla, were less than 8 km deep with moment magnitudes mostly between 1 and 3 and an azimuthal range between 90 and 270°. We used a time window that started at a time that was twice the arrival of the S phase (Aki and Ferrazzini, 2000a; Aki and Chouet, 1975). The coda of the seismogram was instrument corrected before root mean square (RMS) values in 5 s long, non-overlapping windows were calculated (Aki, 1969). We used HEK01 as reference and averaged all RMS values. HEK01 was chosen as reference station as it had the longest seismic dataset and the least local, high-frequency noise given its low elevation and a more sheltered location. RMS values were discarded if a regional event was time-coincident with a local Hekla microseismic event in the corresponding frequency band. The site correction factors are given in table 1.
After applying site corrections a grid search assuming body and surface wave propagation was performed. The grid was a rectangular cuboid extending 7 km east-west, 9 km north-south and from sea level up to 1500 m a.s.l. For the grid search we assumed a surface wave velocity of 1.8 km/s and a shear wave velocity of 2.0 km/s. Based on the results from our sensitivity tests (see paragraph 2 in 5.2) we assumed a quality factor of 100. As a comparison, on Piton de la Fournaise volcano shear wave velocities of 2.3 km/s and quality factors of 50 (Battaglia and Aki, 2003) or shear wave velocities of 1.0 km/s and quality factors of 170 (Taisne et al., 2011) were used for locations. The resulting $\beta \cdot Q$ products are consistent with ours and give the least event location scatter based on our sensitivity test (see 5.2). Each grid point was then compared to a topographic map, all points above the topography were excluded and the remaining grid point with the lowest percentage error was picked as the source. Because other studies (e.g.Pálmason (1971)) found lower seismic velocities that might seem more appropriate in shallow volcanic environments, we show locations for a lower quality factor and seismic velocity in the Appendix.

5.2 Synthetic Tests

The accuracy of the method has been tested previously on visible rockfall, tremor from an eruptive fissure and on a hybrid event and compared with a travel-time location method. For details see Battaglia and Aki (2003), Taisne et al. (2011) and Battaglia et al. (2005), respectively. Locations assuming body and surface waves were similar with better locations for body waves located in the 5 - 10 Hz band (Battaglia and Aki, 2003).
We tested the sensitivity of the intensity method with respect to seismic velocity and quality factor using five type 1 events. The seismic velocities varied between 1 km/s and 4 km/s and the quality factors from 40 to 200. The influence on the locations was only slight and seems to be best for a $Q \cdot \beta$ product of 180 km/s. For higher values the improvement is negligible, for lower values the scattering of the locations increases.
In order to try to further quantify the effects of station geometry we performed synthetic tests assuming a source in a homogeneous, isotropic medium. The amplitudes of the signal at the seismometers were calculated for body waves using the formula from (Battaglia and Aki, 2003) describing the amplitude decrease with respect to distance:

$$A(r_i) = \frac{A_0}{r_i} \cdot e^{-\frac{\pi \cdot f}{Q \cdot \beta} \cdot r_i} \tag{5.3}$$

For the forward calculations of the amplitudes a frequency band of 7 to 10 Hz, a quality factor of 100, a seismic velocity of 2.0 km/s consistent with the above mentioned inversion settings and an arbitrary amplitude at the source A_0 of 2000 for body waves were assumed. A 6 s long Gaussian wavelet sampled at a rate of 100 Hz was used as the source. The synthetic seismograms at the five Hekla stations were then inverted in the 4 - 7 Hz and 7 - 10 Hz band assuming β=2.0 km/s when considering body waves and β=1.8 km/s when considering surface waves and a quality factor of 100 (figure 5).

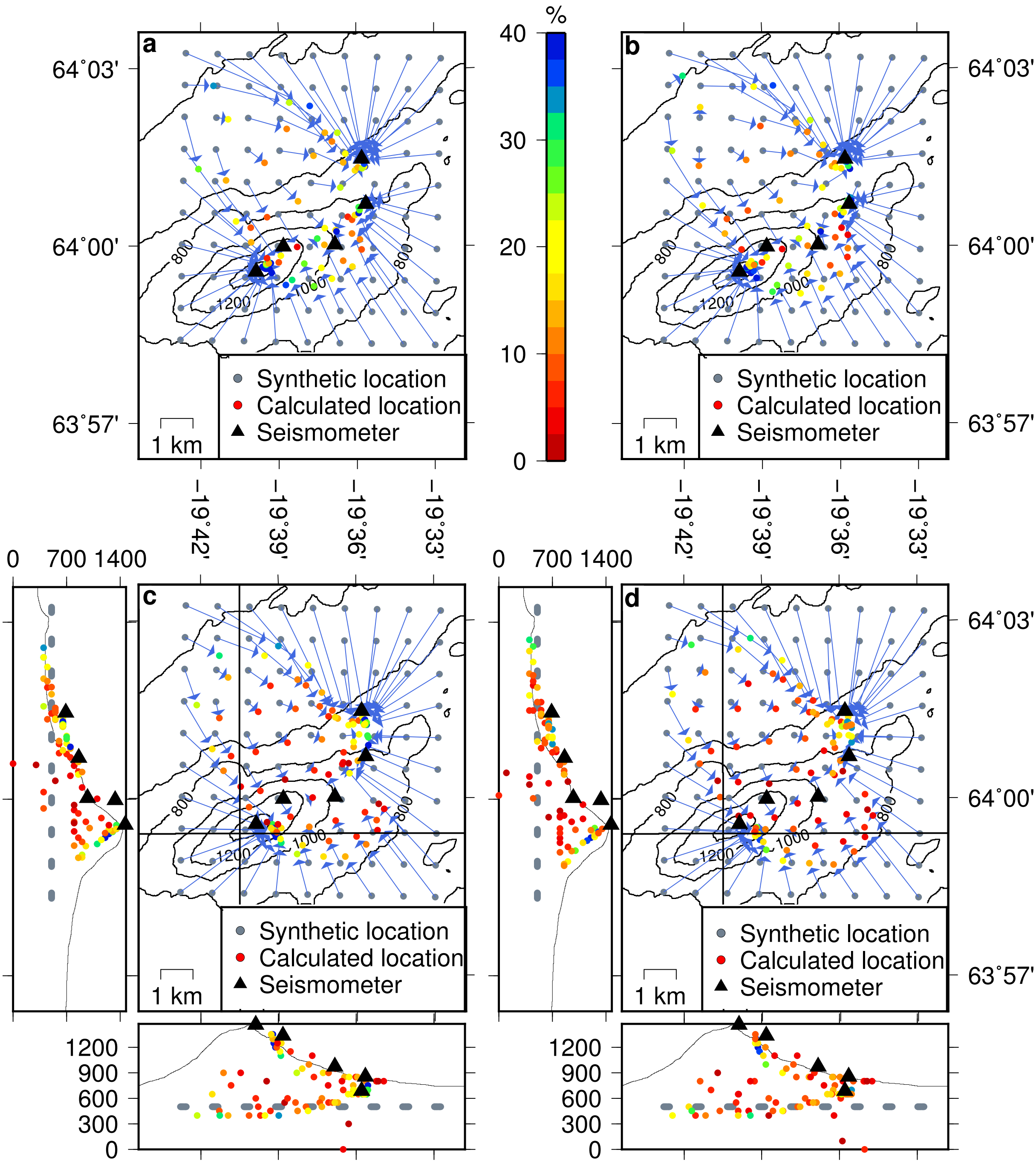

Figure 5: Synthetic tests of the intensity location method on a dataset created with a Gaussian pulse as source travelling as body waves. The plots show the locations of the original sources in grey and the locations of the best fitting source linked with a blue arrow. The best fitting sources are marked with a colored point according to their error percentage. The straight black lines indicate the location of the cross sections. The intensity location method was performed (a) in the 4 - 7 Hz band assuming surface waves, (b) in the 7 - 10 Hz band assuming surface waves, (c) in the 4 - 7 Hz band assuming body waves and (d) in the 7 - 10 Hz band assuming body waves.

The initially rectangular grid of sources at 500 m elevation was extending 2 to 3 km farther in each direction than the stations at the lowest/ highest latitude/ longitude. Our tests reveal that due to our station configuration (which were designed with a focus on event detection but not location) the general locations migrate systematically towards the stations in the inversion. Grid points northeast and southwest of our stations move the most and cluster near HEK01 and HEK05, respectively. Grid points within or closer to our network migrate significantly less. Most locations stayed at approximately the same depth or migrated to a shallower location.

It is important to note that although points move they remain on the initial side of the stations. That is, an event south of the stations is located south of it, an event north of the stations remains in the north during the location procedure. Exceptions include a location very close to HEK03 where a grid point slightly north of the station migrated slightly south and near HEK02 where an individual grid point in the south migrated to the north. High error percentages of points near HEK01 moreover seem to indicate locations of the real sources northeast of the network, which is where, in fact, they are located.

We tested the quality factor and seismic velocity for recoverability. Quality factors between 10 and 190 (stepsize 10) and seismic velocities between 0.5 km/s and 7 km/s (stepsize 500 m/s) were assumed for a location midway between HEK02 and HEK03 and one location outside the network 3 km north of HEK03. For the summit event between HEK01 and HEK03 the results were closest to the real location for Q=90 and β=2.0 km/s for a varying quality factor and Q=100 and β=2.0 km/s for a varying velocity. For the location outside the network the best locations were Q=100 and β=1.0 km/s for a varying velocity and Q=40 and β=2.0 km/s for a varying quality factor. Those values are slightly lower than the parameters Q=100 and β=2.0 km/s that were used in the forward calculations.

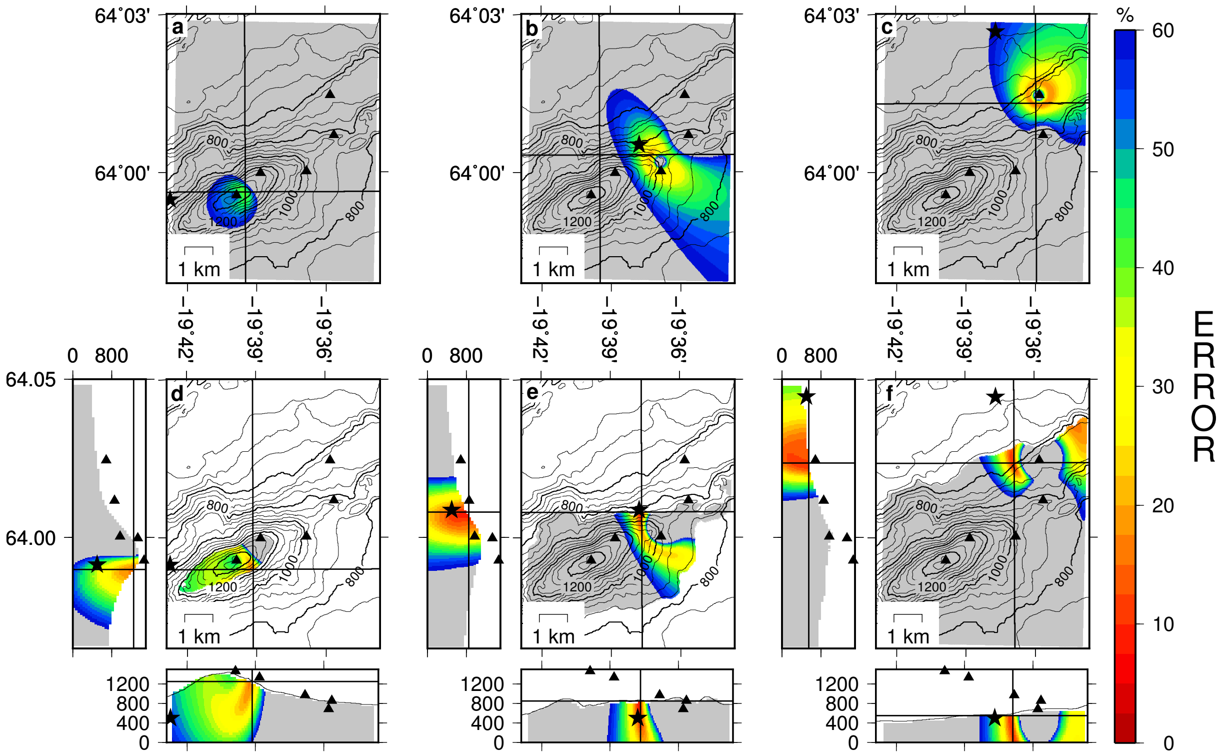

Figure 6: Typical error percentage distributions for three synthetic events. Grey points have errors higher than 60%. All figures show the results in the 7 - 10 Hz band as the figures in the 4 - 7 Hz band were nearly identical. The straight black lines indicate the location of the cross sections and also the location of the point with the lowest error percentage. The black star indicates the original location. The elongation of the error ellipse perpendicular to the line of stations is visible as well as its elongation in depth. (a-c) located assuming surface waves, (d-f) located assuming body waves.

Figure 6 gives an idea of the width and shape of the error in three perpendicular planes through the location of the lowest error percentage. The three representative events were located west of HEK05, northwest of HEK02 and north of HEK01. The grid point with the best fit is marked by the black cross. The plots show the elongation of the lower error percentages perpendicular to the linear trend formed by the deployed stations. The uncertainty in the location is therefore highest in NW-SE direction and in depth. As expected, events at the summit or in the vicinity of the network are well recovered.

6 Location Results

6.1 Locations of the Type 1 Events

The intensity location method was applied to 210 type 1 events for which the start and end times where picked as demonstrated in figures 3a. The total time window was 2 to 8 s long. Locations were estimated in the 4 - 7 Hz band (figure 7) and 7 - 10 Hz band (figure 9).
Most locations cluster around HEK05 and HEK03 which is consistent with the observations that the signals are strongest, shortest and arrive first at these stations. They are also the most constrained events, located in the uppermost 400 m below the summit (800 - 1200 m elevation) slightly north of the main ridge. This clustering of locations is exclusively on the northern flank of the edifice. However, based on our synthetic tests we are confident that this is not an artifact.
The locations near HEK01 have a high error percentage even for the best locations. This might indicate that they occurred outside our station network and moved towards HEK01 as seen in the synthetic tests. The grey points aligning N-S or E-W in the northwestern corner have very high error percentages, occurred outside the grid we set up and follow the edge of the grid.

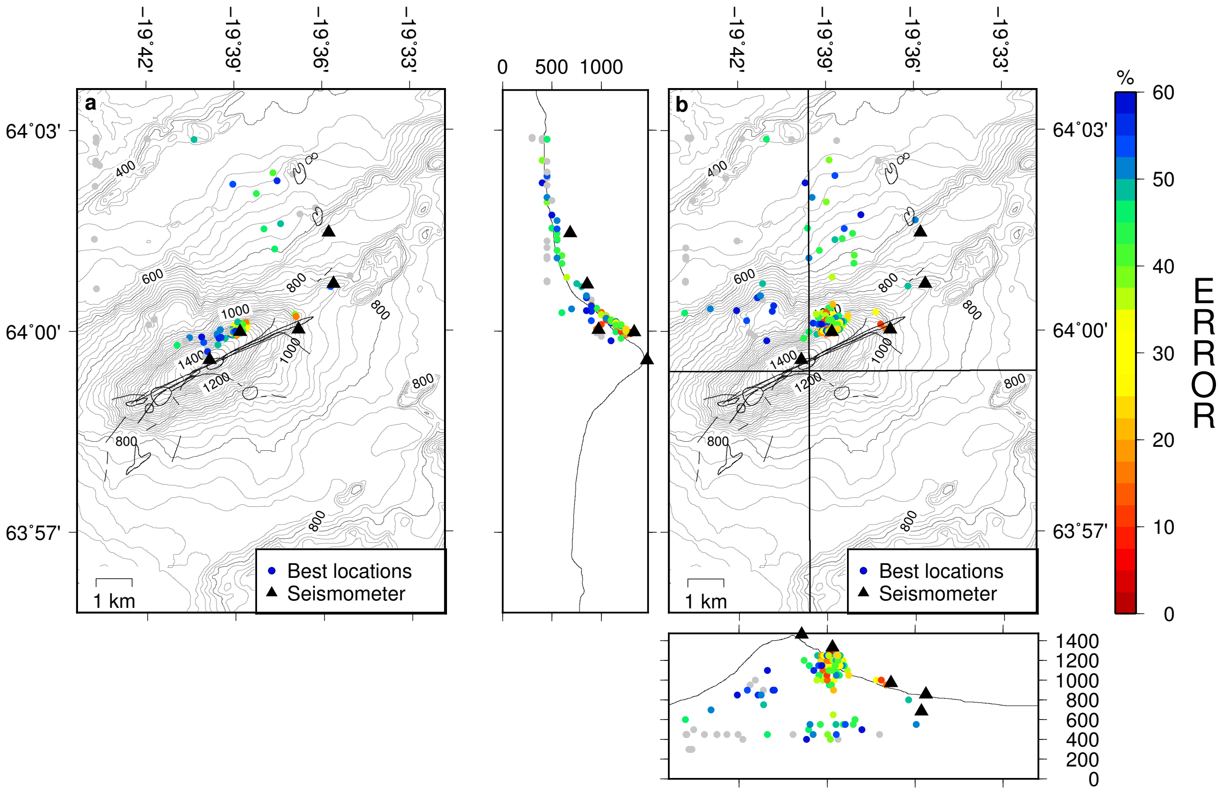

Figure 7: Best fitting locations of 210 type 1 events colored according to the error percentage at the best location. Grey points have errors higher than 60%. Locations are based on the intensity location method in the 4 - 7 Hz band. Each event is represented by one point. Thin black lines indicate the eruptive fissures of the eruptions in 1970, 1980/81, 1991 and 2000. The straight black lines indicate the location of the cross sections. The location method assumed (a) surface waves and (b) body waves.

The error percentage distribution is shown in three dimensions at the best fitting location in figure 8 for two representative events. One event was located at the summit of Hekla (figure 8a) the other one north of it (figure 8b). The uncertainty in depth is visible especially for the event north of the summit. The error ellipse is slightly elongated perpendicular to the line of stations and quite broad northwest of the stations. These results are consistent with the synthetic tests in figure 6.

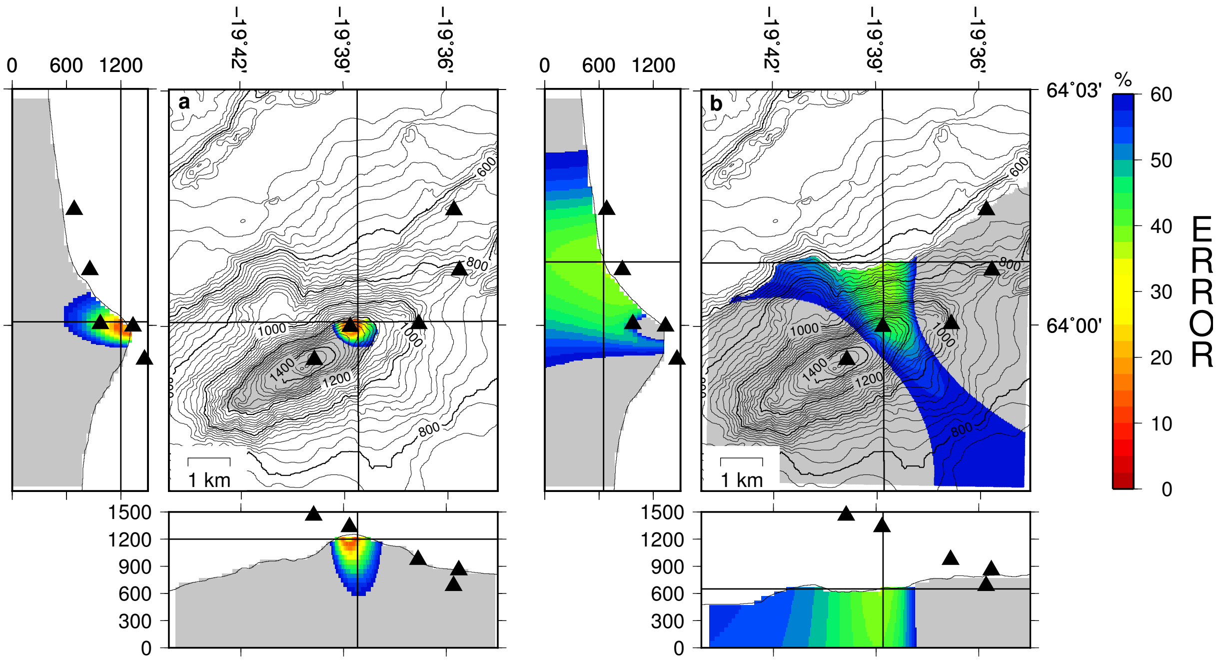

Figure 8: Error percentage distributions for two type 1 events located in the 4 - 7 Hz band assuming body waves. The straight black lines indicate the location of the cross sections as well as the location with the lowest error percentage. The events were located (a) near the summit and (b) northeast of the volcano.

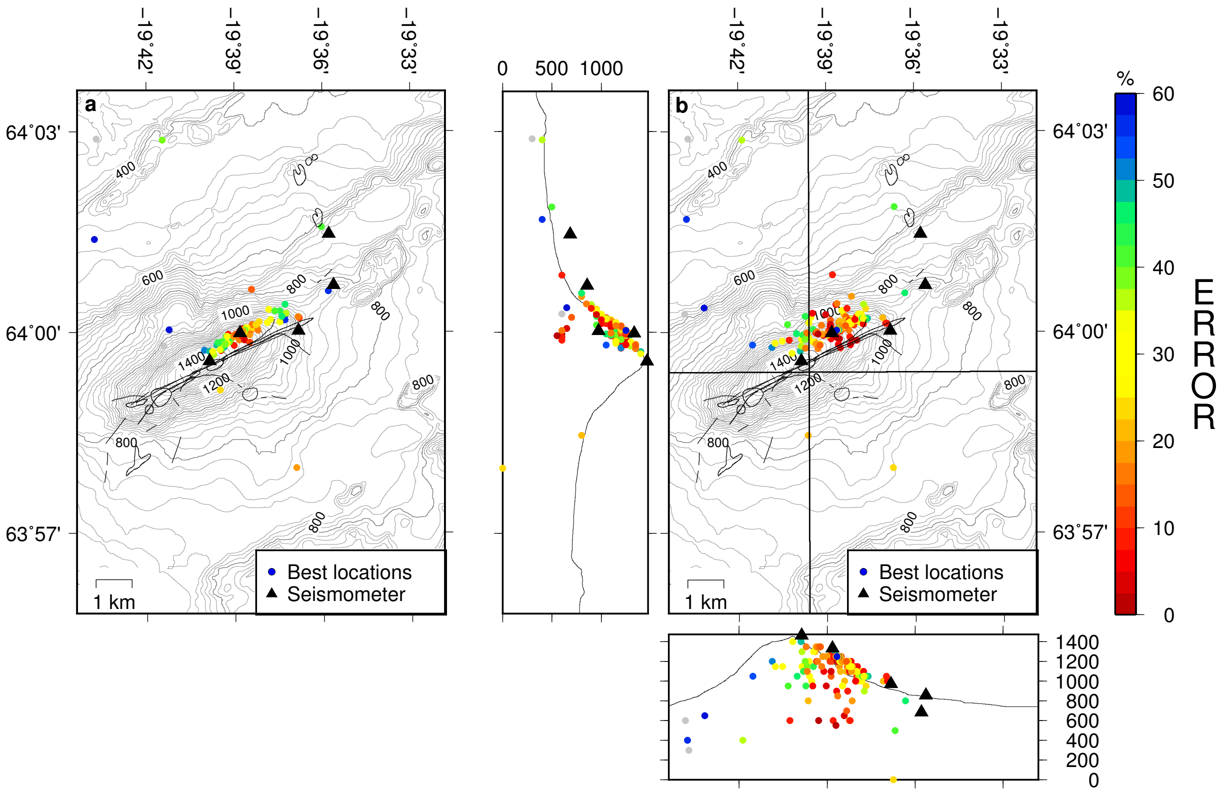

Figure 9: Same as figure 7 except in the 7 - 10 Hz frequency band.

307 In figure 9 we show the same analysis as in figure 7, except for 7 - 10 Hz frequency band.
308 Here the locations have lower error percentages and are more clustered along the northern

flank, than the locations for the 4 - 7 Hz band. This is consistent with observations of Kumagai et al. (2010) that amplitude based location methods perform better for higher frequency data, where the wavefield is more isotropic through wave scattering.

6.2 Locations of the Type 2 Events

Forty type 2 events were located with overall window lengths of 12 to 25 s as indicated by the red lines in figure 4a. As the S/N ratio is better in the 4 - 7 Hz band (see figure 4) we only show the result in this band (figure 10).
The type 2 events are mostly located northwest of HEK01 beyond the flank of Hekla at 400 to 600 m elevation. A few events were located near the summit and have a slightly higher error percentage. It is possible that these events are a mis-classification of type 1 events. Error percentages are comparable to the type 1 events and are slightly lower in the 7 - 10 Hz band.
The type 2 events seem to occur outside our network and might therefore have high error percentages. A comparison to our synthetic tests shown in figure 5 suggests that they occur northeast of our stations and their apparent locations cluster near HEK01 due to our station geometry. They have nevertheless a different character than type 1 events and clearly have a different location, likely to the northeast of Hekla.

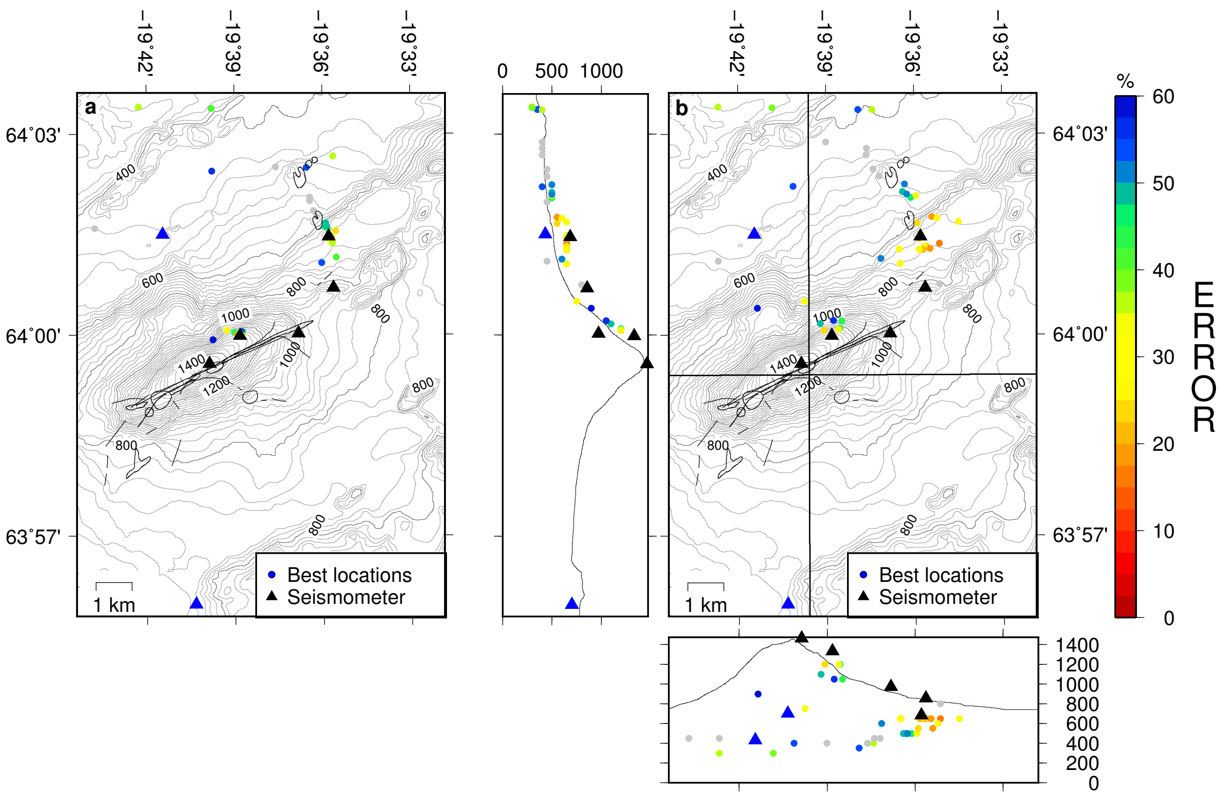

Figure 10: Same as figure 7 but for 40 type 2 events. Locations of the two closest temporary IMO stations marked by blue triangles.

A subset of 19 of these events was located using our five stations and the two additional temporary IMO stations (blue triangles in figure 10). Events in the east moved further eastwards away from the station network. Events north of the network moved towards the stations and westwards or stayed where they were. In fact the locations were consistent with two arrival-time located type 2 events. See section 7 for the methodology. We conclude that the IMO stations help to constrain locations and support our previous suggestion that most of these events occurred outside the network. Although they also suggest that some of them actually occurred west of the volcano in a greater distance.

7 Arrival-Time Location Method

For 23 type 1 events we picked P wave arrival times on all five stations and therefore were able to apply an arrival-time location method. The remaining 187 of the events were emergent or had high noise levels masking the onset. We expect P waves to arrive first and chose a P wave velocity of 2.0km/s $\cdot\sqrt{3} \approx 3.4$ km/s based on our shear wave velocity. Relative arrival-times T_{syn} from each grid point were compared with observed arrival-times T_{obs} for grid points below the topography. The error percentage RES was calculated and the minimum in the grid picked as best fitting location (Battaglia et al., 2005):

$$RES = 100 \cdot \sqrt{\frac{\sum_i (T_{syn} - T_{obs})^2}{\sum_i (T_{obs})^2}} \tag{7.1}$$

The locations from the arrival-time location method are shown in figure 11a. They are broadly consistent with the locations from the intensity location method for the same events (figure 11b). Using the arrival-time location method the locations are about 500 m further east, slightly more scattered and were located a few hundred meters deeper. They also support the observation that the locations are north of the summit fissure on the northern flank of Hekla. The error percentage distribution in figure 12 clearly shows the error in the NW-SE direction and in depth.

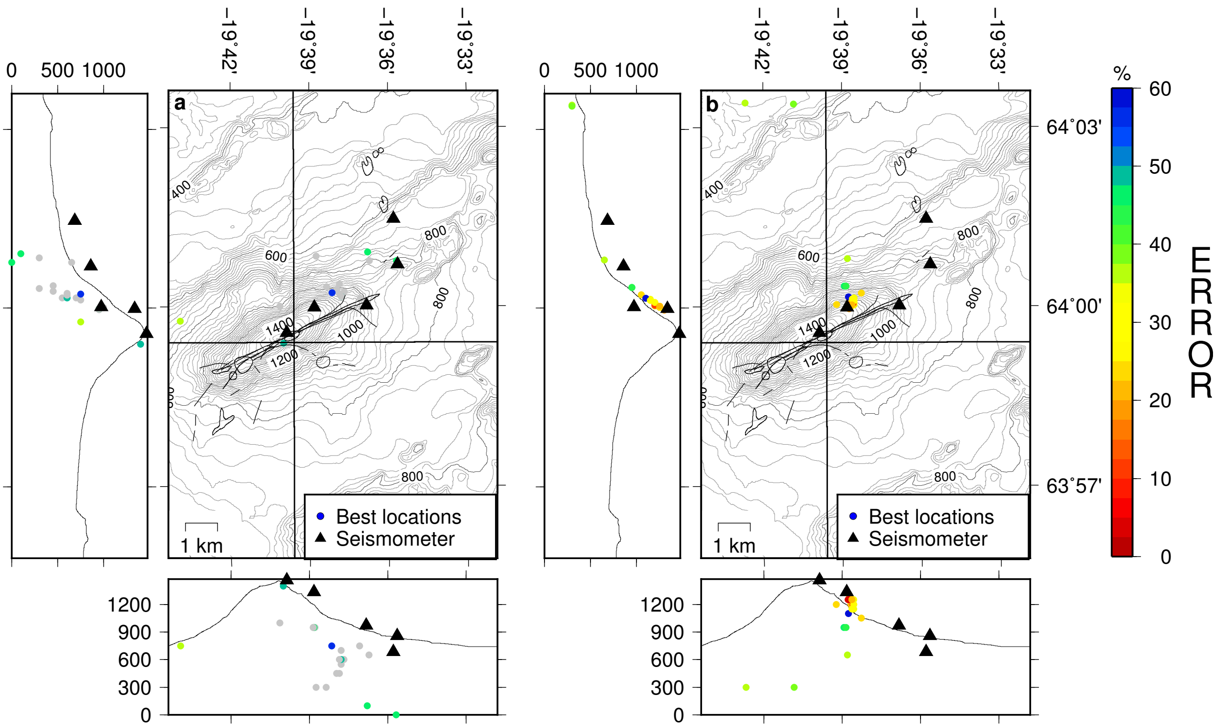

Figure 11: Arrival-time locations of 23 type 1 events (a) in comparison to the results from the intensity location method (4 - 7 Hz) (b). Note the higher error percentages and the locations north of the central fissure at Hekla for the arrival-time locations.

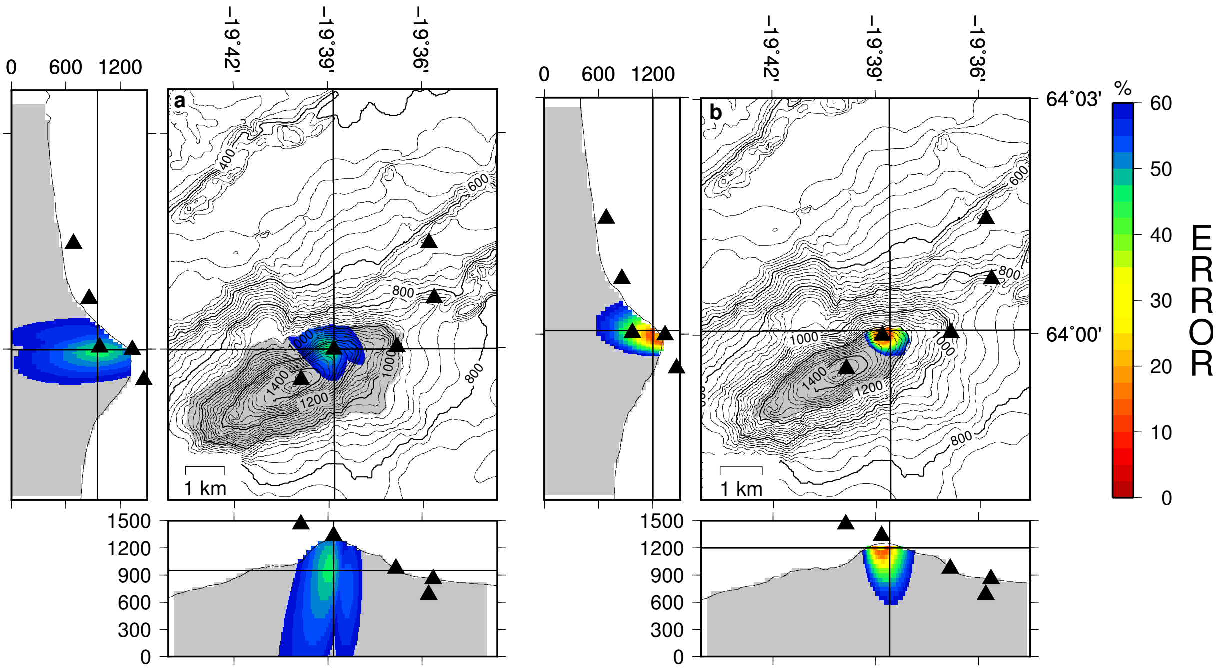

Figure 12: Typical error percentage distribution for a sample location calculated using arrival-times (a) and the corresponding error percentages for the same event located with the intensity location method (b). The straight black lines indicate the location of the cross sections as well as the location with the lowest error percentage.

8 Qualitative Estimates of Event Magnitudes

The regional events used to calculate site correction factors were also used to estimate the size of type 1 and type 2 events. 50 regional events were instrument and site corrected and filtered to the 4 - 7 and 7 - 10 Hz band. The maximum of the smoothed Hilbert Transform was used as maximum amplitude A_i at station i. The amplitude at the source A0 was then calculated for all five stations based on (Battaglia and Aki, 2003):

$$A0_i = \frac{A_i \cdot r_i}{e^{-\frac{\pi \cdot f}{Q \cdot \beta} \cdot r_i}}, r_i = \sqrt{x^2 + y^2 + z^2} \tag{8.1}$$

We assumed $\beta = 2000$ m/s for body waves, $Q = 100$ and calculated the distance based on UTM coordinates of the Hekla stations and the IMO catalogue earthquake locations. A linear regression was then performed with the logarithm of the mean or median of the amplitudes at the source and the published magnitudes (dashed line, figure 13). The amplitudes at the source of type 1 and type 2 events were calculated similarly using the best fitting source location. These amplitudes were then converted to a magnitude using the regression line determined for the regional events (figure 13).

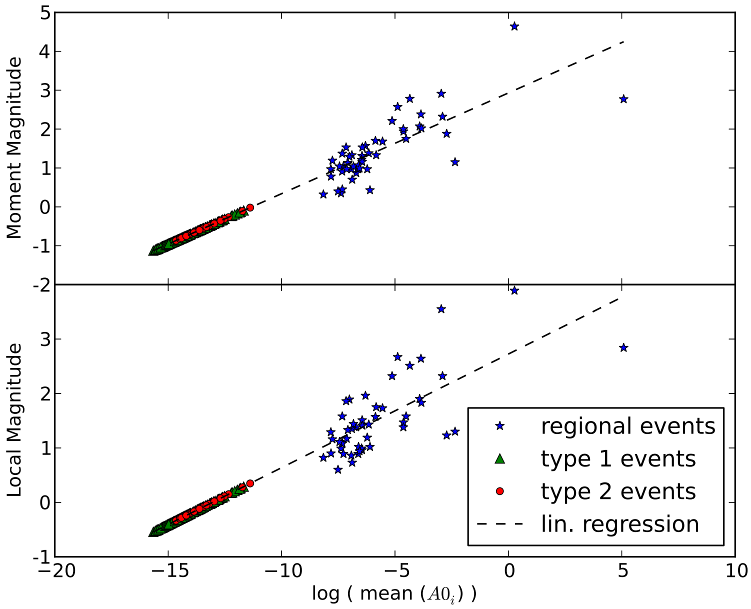

Figure 13: Moment and local magnitudes for type 1 and type 2 events were estimated based on a linear regression of the magnitudes of regional events and the mean amplitudes at the source derived from an amplitude location method.

The moment magnitudes of the regional events were 0.32 to 4.64, the local magnitudes 0.6 to 3.89. As we assumed a straight wave propagation we underestimate A0 for regional events which implies that the magnitudes of type 1 and type 2 events will be overestimated. A0 for type 2 events might be underestimated as well if they actually lie outside our network. Despite the many assumption underlying this qualitative analysis it is clear that type 1 events are smaller than type 2 events. Estimated moment magnitudes are M_W = -1.1 to -0.1 for type 1 and M_W = -0.9 to -0.0 for type 2 and local magnitudes M_L

= -0.5 to +0.3 for type 1 and M_L = -0.3 to +0.3 for type 2 events. The influence of the frequency band and the mean or median is insignificant.

9 Discussion and Conclusions

The type 1 events which were located near the summit of Hekla have significantly lower error percentages at the best fitting location and cluster more than the type 2 events near HEK01 off the flank. The amplitude based locations of 23 of those events chosen because they have sharp onsets, are consistent with their arrival-time locations. According to our synthetic tests some of the events clustering near HEK05 at the summit might have occurred further south or further west. The locations near HEK01 have likely occurred further north or further east. Thus, the cluster visible near HEK01 is most probably an artificial cluster caused by the station geometry. Importantly our synthetic tests also reveal that although a point might move towards the stations it still remains on the initial side (either north or south of the station). This implies that all type 1 events likely occur on the northern flank of the volcano, just north of the main eruptive WSW-ENE striking fissure. This result is consistent with tectonic high-frequency events which were located in the uppermost 0 to 4 km north of the 2000 eruptive fissure before the eruption in 2000 (see figure 5a in Soosalu et al. (2005)). A Synthetic Aperture Radar (SAR) study revealed that shortly before this eruption the surface south of the eruptive fissure was deformed upwards and north of it downwards. The SAR displacement was modelled with a strike-slip fault reaching down to 5.8 km below sea level at a dip of 70-73° SE (Ofeigsson et al., 2011). Another interesting feature is visible when comparing the gradient in figure 1b with the type 1 event locations near the summit in figure 7. The northern flank of Hekla is slightly steeper than the southern flank and the locations cluster in the steepest region north of HEK03 when body waves are assumed and in the steepest regions north of HEK05 and HEK03 if surface waves are assumed. This suggests that edifice stability might play a role in the generation of these events. Seismic signals will in this case be created by minor failures on near surface edifice faults.

The type 2 events cluster mostly in a northwest-southeast striking line near HEK01. Based on synthetic tests we expect that the clustering of events near HEK01 is not real and that they are likely located farther to the NE. This is consistent with the high error percentages, obtained for individual type 2 seismic events. However, the location of the cluster of those events is consistent with the locations of a previous tectonic, high-frequency event swarm. The swarm occurred in the uppermost 3 km in the first three months after the eruption in 1991 that was thought to be linked to a dike intrusion in that region (see figure 2 in Soosalu et al. (2005)). Between 1991 and 2000 some tectonic, low-frequency events occurred in the same region. In Soosalu et al. (2005) figure 2 also shows faults oriented in NNW-SSE and SW-NE direction near HEK01 that might be a possible source of earthquakes.

Based on their frequency content and seismogram envelope shapes (diffuse-like), we interpret type 2 events as tectonic (or volcano-tectonic) in nature, suffering strong path effects. Although they are poorly located we are confident that they lie some distance away, outside our network. As they propagate they will be affected by attenuation and scattering effects which might hide a type 1 like event of slightly bigger magnitude. Type 1 events are clearly brittle-failure (volcano-tectonic like) in nature. Type 1 events locate along a well defined structural trend. This trend mirrors the orientation of Hekla's 2000 eruptive fissure and lies about 200 m to 1 km NNW of its surface expression. This observation combined with their occurrence on the steepest portion of the northern flank of Hekla would suggest that type 1 events are structurally controlled and related to ongoing instability of the northern flank of the volcano.

Since we did not observe diurnal trends in the amount of seismicity we consider ice or temperature changes an unlikely source. If the seismicity is related to magma such shallow location of magma would influence gas, GPS or INSAR measurements as well, none of which was observed. Ongoing summit gas measurements during our seismic experiment were undertaken every six hours for half an hour until September 6^{th} (pers. comm. Evgenia Ilyinskaya, April 2014) but changes were only slight and no correlation with the number of seismic events per day was found.

Although we subdivided the events in two classes we would like to stress that they might be the same type but of different size occurring in different locations. This seems to be supported by our locations and magnitude estimations. In previous eruptions shallow seismicity was detected whilst the magma was still at significant depth but rising towards the surface (Sturkell et al., 2013; Soosalu et al., 2005). Monitoring near summit microseismicity can help further constrain these observations. On Piton de la Fournaise shallow microseismicity is shown to herald the location of future eruptive fissures (Barros et al., 2013).

Our experiment detected a high level of shallow background seismicity primarily on the northern flank near the summit. This seismicity is not detected by the permanent stations of the IMO network as it is below their detection threshold. We demonstrate that permanent stations closer to Hekla could improve the detection threshold of ongoing earthquakes on the volcano. The high levels of background microseismicity at Hekla suggests that the edifice is likely in a state of critical instability. If so, microseismicity levels will be very sensitive to small future stress perturbations associated with magma migration at depth. We suggest that continuous near-summit monitoring of microseismicity levels might offer an earlier indication of imminent eruptions. Currently Hekla switches from apparently quiescent to fully eruptive on the order of only one hour.

10 Acknowledgements

The data were collected and analysed within the framework of FutureVolc, which has received funding from the European Union's Seventh Programme for research, technological development and demonstration under grant agreement No 308377. We thank Baldur Bergsson and Thomas Eyre for support in the field. We are grateful to Ivan Lokmer, Benedikt G. Ofeigsson, Evgenia Ilyinskaya, Páll Einarsson and Jean Battaglia for helpful discussions and comments. We also want to thank Heidi Soosalu and an anonymous reviewer for their critical comments that helped to improve the manuscript.

11 Appendix

Figure 14 shows the locations using the intensity location method assuming a lower quality factor Q=50 (Battaglia and Aki, 2003) and seismic velocity β=1.2 km/s. The latter value is based on a seismic refraction study that found low P wave velocities in a refraction profile north of Hekla (Pálmason, 1971). The influence on the locations is small although the locations scatter more than for higher values (see figure 7b, 9b and 10b). Hence we conclude that for our network geometry the broad locations of the events (on the northern flank of the volcano) are insensitive to the details of velocity and Q structure.

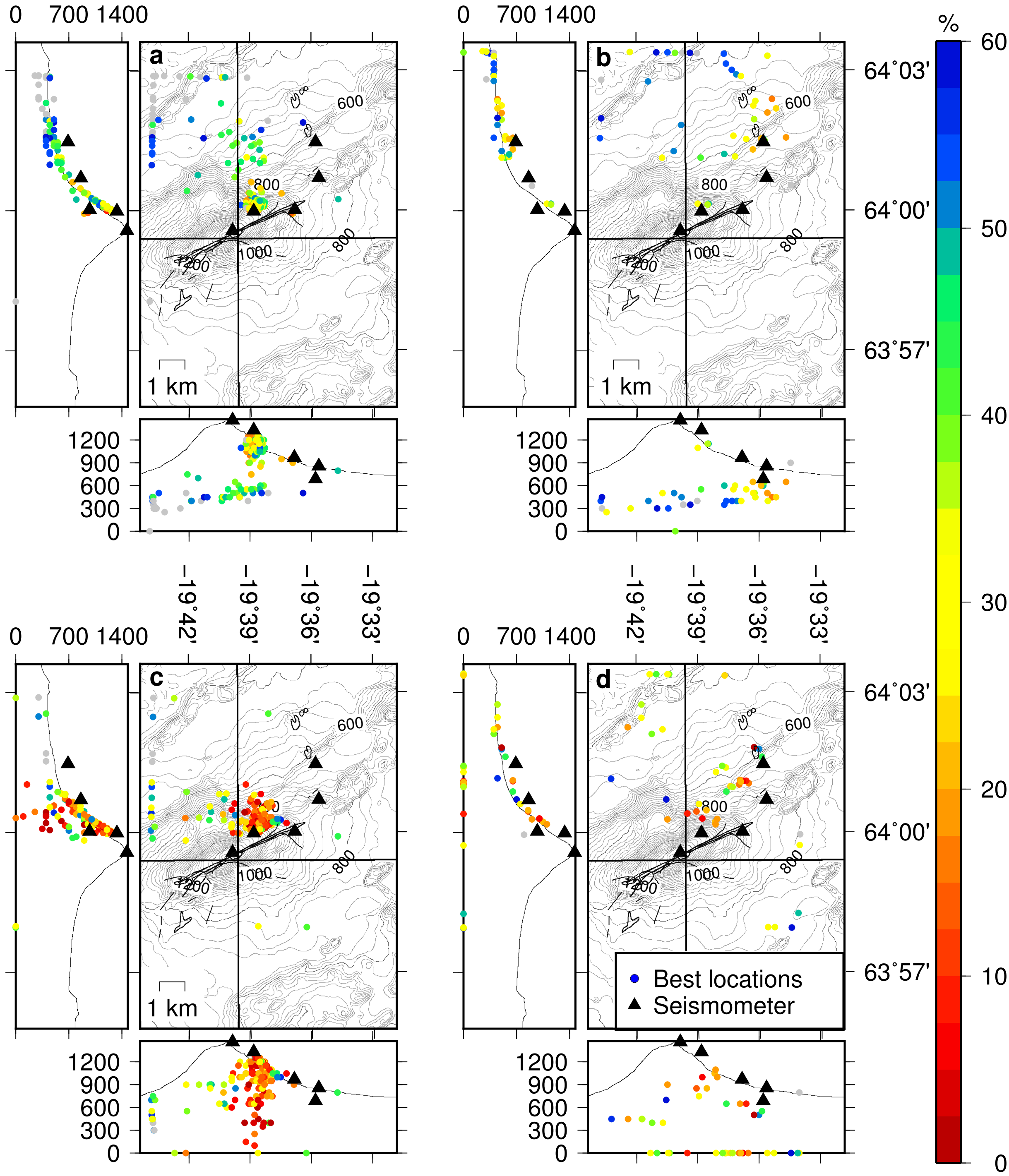

Figure 14: Intensity ratio locations assuming a Q=50 and β=1.2 km/s (a) in the 4 - 7 Hz band for type 1 events (4 - 7 Hz) (b) same as a but for type 2 events (c) same as a but in the 7 - 10 Hz frequency band (d) same as b but in the 7 - 10 Hz frequency band. Note the similarity to the locations with the higher quality factor and velocities.

12 References

Keiiti Aki. Analysis of the seismic coda of local earthquakes as scattered waves. *Journal of Geophysical Research*, 74(2):615–631, 1969. doi: 10.1029/JB074i002p00615.

Keiiti Aki and Bernard Chouet. Origin of Coda Waves: Source, Attenuation, and Scattering Effects. *Journal of Geophysical Research*, 80(23):3322–3342, 1975. doi: 10.1029/JB080i023p03322.

Keiiti Aki and Valérie Ferrazzini. Seismic monitoring and modeling of an active volcano for prediction. *Journal of Geophysical Research: Solid Earth*, 105(B7):16617–16640, 2000a. doi: 10.1029/2000JB900033.

Keiiti Aki and Valérie Ferrazzini. Seismic monitoring and modeling of an active volcano for prediction. *Journal of Geophysical Research: Solid Earth*, 105(B7):16617–16640, 2000b. ISSN 2156-2202. doi: 10.1029/2000JB900033.

Louis De Barros, Christopher J Bean, Megan Zecevic, Florent Brenguier, and Aline Peltier. Eruptive fracture location forecasts from high-frequency events on Piton de la Fournaise Volcano. *Geophysical Research Letters*, 40(17):4599–4603, 2013. doi: 10.1002/grl.50890.

Jean Battaglia and Keiiti Aki. Location of seismic events and eruptive fissures on the Piton de la Fournaise volcano using seismic amplitudes. *Journal of Geophysical Research*, 108 (B8):2364, 2003. ISSN 0148-0227. doi: 10.1029/2002JB002193.

Jean Battaglia, Keiiti Aki, and Valérie Ferrazzini. Location of tremor sources and estimation of lava output using tremor source amplitude on the Piton de la Fournaise volcano: 1. Location of tremor sources. *Journal of Volcanology and Geothermal Research*, 147 (3-4):268–290, October 2005. ISSN 03770273. doi: 10.1016/j.jvolgeores.2005.04.005.

Páll Einarsson. Earthquakes and present-day tectonism in Iceland. *Tectonophysics*, 189 (1-4):261–279, April 1991. ISSN 00401951. doi: 10.1016/0040-1951(91)90501-I.

Páll Einarsson and Sveinbjörn Björnsson. Seismic activity associated with the 1970 eruption of volcano Hekla in Iceland. *Jökull*, 26:8–19, 1976.

Páll Einarsson and Sveinbjörn Björnsson. Jarðskjáftamælingar á Raunvísindastofnun Háskólans (in icelandic). In Ãđ. Sigfússon, editor, *Í Hlutarins Eðli. Festschrift for Thorbjörn. Sigurgeirsson, Menningarsjóður, Reykjavík*, pages 251–278. Springer-Verlag, 1987.

Halldór Geirsson, Peter LaFemina, Thóra Árnadóttir, Erik Sturkell, Freysteinn Sigmundsson, Matthew Travis, Peter Schmidt, Bjorn Lund, Sigrún Hreinsdóttir, and Rick Bennett. Volcano deformation at active plate boundaries: Deep magma accumulation at Hekla volcano and plate boundary deformation in south Iceland. *Journal of Geophysical Research*, 117(B11), November 2012. ISSN 0148-0227. doi: 10.1029/2012JB009400.

K Grönvold, G Larsen, P Einarsson, S þórarinsson, and K Sæmundsson. The Hekla Eruption 1980-1981. *Bulletin of Volcanology*, 46(4):349–363, 1983. doi: 10.1007/BF02597770.

Agust Gudmundsson, Niels Oskarsson, Karl Grönvold, Kristjan Sæmundsson, Oddur Sigurdsson, Ragnar Stefansson, Sigurdur R Gislason, Pall Einarsson, Bryndis Brandsdottir, Gudrun Larsen, Haukur Johannesson, and Thorvaldur Thordarson. The 1991 eruption of Hekla, Iceland. *Bulletin of Volcanology*, 54(3):238–246, 1992. doi: 10.1007/BF00278391.

Ármann Höskuldsson, Níels Óskarsson, Rikke Pedersen, Karl Grönvold, Kristín Vogfjörð, and Rósa Ólafsdóttir. The millennium eruption of Hekla in February 2000. *Bulletin of Volcanology*, 70(2):169–182, April 2007. ISSN 0258-8900. doi: 10.1007/s00445-007-0128-3.

Allen L. Husker, Vladimir Kostoglodov, Victor M. Cruz-Atienza, Denis Legrand, Nikolai M. Shapiro, Juan S. Payero, Michel Campillo, and Eduardo Huesca-Pérez. Temporal variations of non-volcanic tremor (NVT) locations in the Mexican subduction zone: Finding the NVT sweet spot. *Geochemistry, Geophysics, Geosystems*, 13(3), March 2012. ISSN 15252027. doi: 10.1029/2011GC003916.

Steinunn S Jakobsdóttir. Seismicity in Iceland: 1994 - 2007. *Jökull*, 58:75–100, 2008.

A D Jolly, G Thompson, and G E Norton. Locating pyroclastic flows on Soufriere Hills Volcano, Montserrat, West Indies, using amplitude signals from high dynamic range instruments. *Journal of Volcanology and Geothermal Research*, 118(3-4):299–317, 2002. doi: 10.1016/S0377-0273(02)00299-8.

Hiroyuki Kumagai, Pablo Palacios, Takuto Maeda, Diego Barba Castillo, and Masaru Nakano. Seismic tracking of lahars using tremor signals. *Journal of Volcanology and Geothermal Research*, 183(1-2):112–121, May 2009. ISSN 03770273. doi: 10.1016/j.jvolgeores.2009.03.010.

Hiroyuki Kumagai, Masaru Nakano, Takuto Maeda, Hugo Yepes, Pablo Palacios, Mario Ruiz, Santiago Arrais, Mayra Vaca, Indira Molina, and Tadashi Yamashima. Broadband seismic monitoring of active volcanoes using deterministic and stochastic approaches. *Journal of Geophysical Research*, 115(B8), August 2010. ISSN 0148-0227. doi: 10.1029/2009JB006889.

Alan T. Linde, Kristjan Agustsson, I. Selwyn Sacks, and Ragnar Stefansson. Mechanism of the 1991 eruption of Hekla from continuous borehole strain monitoring. *Nature*, 365: 737–740, 1993. doi: 10.1038/365737a0.

Benedikt G. Ofeigsson, Andrew Hooper, Freysteinn Sigmundsson, Erik Sturkell, and Ronni Grapenthin. Deep magma storage at Hekla volcano, Iceland, revealed by InSAR time series analysis. *Journal of Geophysical Research*, 116(B5):B05401, May 2011. ISSN 0148-0227. doi: 10.1029/2010JB007576.

Guðmundur Pálmason. *Crustal structure of Iceland from explosion seismology.* PhD thesis, Societas Scientiarum Islandica, 40, Reykjavik, 187 pp., 1971.

Heidi Soosalu and Páll Einarsson. Seismicity around the Hekla and Torfajökull volcanoes, Iceland, during a volcanically quiet period, 1991 - 1995. *Bulletin of Volcanology*, 59(1): 36–48, 1997. doi: 10.1007/s004450050173.

Heidi Soosalu and Páll Einarsson. Earthquake activity related to the 1991 eruption of the Hekla volcano, Iceland. *Bulletin of Volcanology*, 63(8):536–544, January 2002. ISSN 0258-8900. doi: 10.1007/s00445-001-0177-y.

Heidi Soosalu, Páll Einarsson, and Bergþóra S. Þorbjarnardóttir. Seismic activity related to the 2000 eruption of the Hekla volcano, Iceland. *Bulletin of Volcanology*, 68(1):21–36, May 2005. ISSN 0258-8900. doi: 10.1007/s00445-005-0417-7.

Erik Sturkell, Kristján Ágústsson, Alan T. Linde, Selwyn I. Sacks, Páll Einarsson, Freysteinn Sigmundsson, Halldór Geirsson, Rikke Pedersen, Peter C. LaFemina, and Halldór Ólafsson. New insights into volcanic activity from strain and other deformation data for the Hekla 2000 eruption. *Journal of Volcanology and Geothermal Research*, 256:78–86, April 2013. ISSN 03770273. doi: 10.1016/j.jvolgeores.2013.02.001.

B. Taisne, F. Brenguier, N. M. Shapiro, and V. Ferrazzini. Imaging the dynamics of magma propagation using radiated seismic intensity. *Geophysical Research Letters*, 38 (4), February 2011. ISSN 00948276. doi: 10.1029/2010GL046068.

S Thórarinsson, S Steinthórsson, T Einarsson, H Kristmannsdóttir, and N Oskarsson. Eruption on Heimaey, Iceland. *Nature*, 241(5389):372–375, 1973. doi: 10.1038/241372a0.